Josephson tunnel junctions with a strong ferromagnetic interlayer

A. A. Bannykh
Institute of Solid State Research and JARA-Fundamentals of Future Information Technology, Research Centre, Jülich, 52425 Jülich, Germany
and Institute of Solid State Physics, Russian Academy of Sciences, Chernogolovka, 142432, Russia

J. Pfeiffer
Physikalisches Institut-Experimentalphysik II and Center for Collective Quantum Phenomena, Universität Tübingen, Auf der Morgenstelle 14, 72076 Tübingen, Germany

V. S. Stolyarov, I. E. Batov, and V. V. Ryazanov
Institute of Solid State Physics, Russian Academy of Sciences, Chernogolovka, 142432, Russia

M. Weides*
Institute of Solid State Research and JARA-Fundamentals of Future Information Technology, Research Centre, Jülich, 52425 Jülich, Germany

(Received 25 August 2008; revised manuscript received 16 December 2008; published 2 February 2009)

The dependence of the critical current density j_c on the ferromagnetic interlayer thickness d_F was determined for $Nb/Al_2O_3/Cu/Ni/Nb$ Josephson tunnel junctions with ferromagnetic Ni interlayer thicknesses from very thin films (~ 1 nm) upward and classified into F-layer thickness regimes showing a dead magnetic layer, exchange, exchange+anisotropy and total suppression of j_c. The Josephson coupling changes from 0 to π as function of d_F, and—very close to the crossover thickness—as function of temperature. The strong suppression of the supercurrent in comparison to nonmagnetic $Nb/Al_2O_3/Cu/Nb$ junctions indicated that the insertion of a F layer leads to additional interface scattering. The transport inside the dead magnetic layer was in dirty limit. For the magnetically active regime fitting with both the clean and the dirty limit theories was carried out, indicating dirty limit condition, too. The results were discussed in the framework of literature.

DOI: 10.1103/PhysRevB.79.054501 PACS number(s): 74.25.Fy, 74.50.+r, 85.25.Cp

I. INTRODUCTION

The combination of superconducting (S) and ferromagnetic (F) materials in layered structures leads to phase oscillations of the superconducting wave function inside the ferromagnet.[1] If the F-layer thickness d_F in SFS Josephson junctions (JJs) is of the order of one-half of this oscillation wavelength, the wave function changes its sign, i.e., shifts its phase by π while crossing the F layer. In this case the critical current I_c (and critical current density j_c) turns out to be negative and the current-phase relation reads $I=I_c\sin(\phi)=|I_c|\sin(\phi+\pi)$ with $I_c<0$, ϕ being the phase difference between the two superconducting electrodes. Such JJs are called π JJs because their phase difference is $\phi+\pi$ in the ground state.[1] Conventional JJs are called 0 JJs because they have a current-phase relation of $I=I_c\sin(\phi)$ with $I_c>0$ and the ground phase difference $\phi=0$. The insertion of an insulating barrier I in SFS stacks, i.e., SIFS stacks, is advantageous as the damping of Josephson phase dynamics becomes lower and the voltage drop gets larger. This facilitates both the study of dynamics and the transport measurements.

The most convincing demonstration of the phase oscillations in SFS/SIFS structures is the *damped oscillatory behavior* of the critical current I_c in the F layer as a function of temperature T (Refs. 2 and 3) or of the F-layer thickness d_F.[4–6] The decay length is ξ_{F1} and the oscillation period is $2\pi\xi_{F2}$, where ξ_{F2} is the imaginary part of the complex coherence length. ξ_{F1} is based on the well-known proximity effect, i.e., the exponential decay of the Cooper pair density inside a metal adjacent to a superconductor. A quantitative model in the *dirty limit* where the mean-free path $\ell<d_F$ and $\ell<\hbar v_F/E_{\mathrm{ex}}$, with v_F being the Fermi velocity, E_{ex} being the magnetic exchange energy, can be found in Ref. 7. This model utilizes parameters which characterize the material properties of the S and F layers and the S/F interface transparency. At $T\lesssim T_c\ll E_{\mathrm{ex}}/k_B$

$$I_c(d_F)\sim\exp\left(\frac{-d_F}{\xi_{F1}}\right)\cos\left(\frac{d_F-d_F^{\mathrm{dead}}}{\xi_{F2}}\right), \tag{1}$$

where

$$\xi_{F1,F2}=\sqrt{\frac{\hbar v_F\ell}{3E_{\mathrm{ex}}}}\left(\sqrt{\sqrt{1+\underbrace{\left(\frac{\hbar}{E_{\mathrm{ex}}\tau_m}\right)^2}_{\to 0}}\pm\frac{\hbar}{E_{\mathrm{ex}}\tau_m}}\right)^{-1}$$
$$\approx\sqrt{\frac{\hbar v_F\ell}{3E_{\mathrm{ex}}}}\left(1\pm\frac{\hbar}{2E_{\mathrm{ex}}\tau_m}\right)^{-1}.$$

The parameter $\hbar/E_{\mathrm{ex}}\tau_m$ is considered as being much smaller than unity. τ_m is the inelastic magnetic scattering time and d_F^{dead} the magnetic dead layer thickness. Within the framework of this theory ξ_{F1} is shorter than ξ_{F2}. Strictly speaking, Eq. (1) is only valid close to $T_c\approx 9$ K for Nb-based JJs,

whereas most of our samples were measured at 4.2 K. However, the $I_c(d_F,T)$ dependence with an arbitrary temperature T is a complex sum depending on Matsubara frequencies, spin-flip scattering time and exchange energy. It was shown in Ref. 5 that the corrections originating from this complex approach are important only for calculations of $I_c(T)$ dependencies close to the 0 to π transition points. The approach used in Eq. (1) yields good results being suitable for fitting of $I_c(d_F)$ dependencies in a wide temperature range.

Experimentally for JJs in dirty limit[5,6] not more than two oscillations of $I_c(d_F)$ were observed. Below T_c the temperature variation in E_{ex} is negligible for $E_{ex} \gg k_B T$ and $I_c(T)$ depends mostly on the temperature-sensitive effective magnetic scattering rate. For example, temperature-driven changes in the coupling were observed in Refs. 3, 5, and 6.

On the contrary, in the *clean limit*, where $\ell > d_F$, the simple clean limit theory for T near T_c (Ref. 1) is

$$I_c(d_F) \sim \frac{\sin\left[\frac{2E_{ex}}{\hbar v_F}(d_F - d_F^{dead})\right]}{\frac{2E_{ex}}{\hbar v_F}(d_F - d_F^{dead})}. \quad (2)$$

The decay of $I_c \sim 1/d_F$ can be much slower than its oscillation period. As a consequence, several phase oscillations may be experimentally detectable. For example, multiple $I_c(d_F)$ oscillations were possibly observed in SFS JJs using elemental magnets such as Ni.[8–11] Unfortunately, insufficient density of data points has not allowed to carry out a reliable quantitative comparison between theory and experiment. Although the absolute $I_c(d_F)$ dependencies for all sets[8–11] of *clean* Ni-SFS junctions are hardly comparable, as a general feature the decay of adjacent maxima amplitudes is below a factor of 4–5, much smaller than the observed factor of 10^4 as it is the case with *dirty* NiCu-SFS junctions.[5] SIFS stacks in the clean limit may be used to obtain a high critical current density j_c in the π state, which, for example, is advantageous to obtain $0-\pi$ junctions[12,13] in the long Josephson limit and to study the dynamics of fractional vortices.[14]

The clean limit theory from Ref. 1, i.e., Eq. (2), yields no temperature driven 0 to π transition for $E_{ex} \gg k_B T$ and temperature-independent E_{ex}. A more complex theory[15] for strong magnets (such as Ni) and insulating interfaces, i.e., tunnel barriers, predicts that samples with d_F very close to the crossover thickness $d_F^{0-\pi}$ may change their ground state with temperature. However, up to now, a temperature-driven phase transition for JJs in the clean limit or for SFS-type JJs with elemental magnetic interlayer was not reported yet.

Diluted magnetic alloys (CuNi, PdNi) contain numerous spin-flip centers (e.g., Ni-rich clusters) that increase superconducting order-parameter decay. So the elemental magnet use in SIFS junction can yield some advantages. In this paper, we study Ni-SIFS junctions starting with $d_F \sim 1$ nm upward and a high density of data points along the $j_c(d_F)$ dependence. In particular, we show details of the Fraunhofer pattern $I_c(H)$ of these junctions and their $I_c(T)$ dependence for various thicknesses. The results are divided into two parts: Sec. II addresses the fabrication, $j_c(d_F)$, $I_c(T)$ and $I_c(H)$ measurements and in Sec. III we discuss our results using the transport theories in clean and dirty limit and compare it with literature.

II. EXPERIMENT

To produce high quality SIFS JJs one has to control both thickness and interface roughness of the F layer on a subnanometer scale. The multilayers were computer-controlled sputter deposited at room temperature at a background pressure of 5×10^{-7} mbar on 4 in. wafers. The uniform growth of the Ni layer was ensured by a thin 2 nm Cu interlayer between the I layer (necessarily having flat interfaces) and the F layer.[17] Thus, the stack was actually SINFS-type. The presence of Cu does not influence much the current-voltage curves (IVC) as determined by SIS- and SINS-type junctions, due to the strong proximity effect of Cu. The Nb electrodes had thicknesses of 150 nm (bottom) and 400 nm (top). Anodic oxidation spectroscopy on reference SIS samples, x-ray diffraction (XRD), and profiler measurements of the sputter rates and specific resistance measurement of Nb thin films have been made to control the quality of films. The Nb bottom electrode was made up by four 37 nm Nb layers, each separated by 2.4 nm Al layers to reduce the total roughness.[18] One wafer contained JJs with different d_F deposited in a single run by shifting the substrate and the Ni-sputter target.[17] The estimation of the F-layer thickness d_F yields values which do not reflect the finite diameter of Ni atoms, but the polycrystalline growth of F layer may thoroughly permit a steady change in the *effective* F-layer thickness by delicate variation in the sputtering rate. A systematic, absolute error in d_F due to an off-centered wafer during deposition is minimized by a special wafer clamp. The relative error due to a nonideal wedge-shaped F layer (having two gradients, one parallel, and a much smaller one perpendicular to the wafer axis) was minimized by taking JJs being located maximally ca. 1 mm apart the wafer axis. We estimate the relative error in d_F as less than 5%. The Al_2O_3 tunnel barrier was formed statically (5 mbar partial oxygen pressure, set 1) or dynamically (0.017 mbar, set 2) for 30 min at room temperature. The JJs had areas of 30×30 and 100×50 μm^2. The lateral sizes of these junctions were comparable or smaller than the Josephson penetration length λ_J. The transport measurement, i.e., $I_c(H)$ and IVC, gave no indication of the existence of a superconducting short neither inside the Al_2O_3 tunnel barrier nor in the insulating Nb_2O_5 barrier.

The samples were cooled down using μ-metal or cryoperm shields to suppress stray fields. Transport measurements were performed in liquid He either using a dip stick setup or a cryostat with the respective inset. The cryostat could reach temperatures between 1.3–10 K. Standard room-temperature voltage amplifiers were used. A magnetic field H was applied in-plane and parallel to the longer sample axis (regarding the 100×50 μm^2 samples). The current bias was computer-controlled statically swept while measuring the voltage drop across the junction. Both current and voltage values were automatically averaged over several hundreds of data points for each step. The upper limit of I_c was determined by a given voltage criteria.

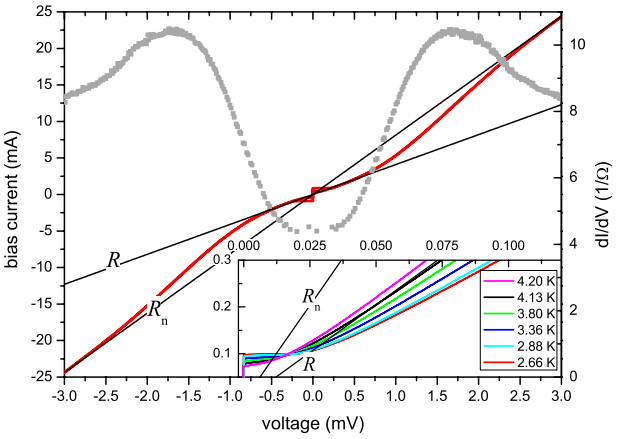

FIG. 1. (Color online) (a) Current-voltage curves and dI/dV characteristics (square symbols) at 4.2 K of d_F=1.4 nm sample. The inset depicts IVC for d_F=2.6 nm. Both the normal and subgap resistances R_n and R are plotted (gray lines).

The IV and dI/dV characteristics (square symbols) at 4.2 K of d_F=1.4 nm sample together with the temperature dependence of IVC for d_F=2.6 nm sample are plotted in Fig. 1. The data close to 0 μV are removed from the dI/dV graph. The maximum conductivity appears for voltages close to the superconducting gap (1.7 mV) of the bottom electrode. The gap of the top electrode is covered by the large subgap current in F layer. Both the normal and subgap resistances R_n and R are plotted (black lines).

Figure 2 depicts the $j_c(d_F)$ dependencies for both sets of samples. Note the logarithmic scale of the j_c axis. The generally larger j_c's for set 2 reflect the thinner Al_2O_3 tunnel barrier than in set 1. Samples with $d_F \lesssim 2.0$ nm showed an underdamped behavior, i.e., a hysteretic IV curve, at 4.2 K (data not shown). Normal state and subgap resistance indicate a small variation (~5%) for JJs with the same d_F. All JJs up to d_F=3.8 nm (solid symbols) had standard $I_c(H)$ pattern [see Figs. 3(a) and 3(b)] and showed a small junction to junction variation in j_c (~5%). Between d_F =3.8–4.4 nm (☆ in Fig. 2) the JJs had strongly shifted $I_c(H)$ pattern, as depicted in Fig. 3(c); the magnetic origin due to anisotropy effects was discussed in Ref. 16. For the respective fitting procedure for each d_F only the largest I_c's, measured at finite H, were used. For $d_F > 4.4$ nm no $I_c(H)$ pattern could be measured, as no dependence on applied magnetic field was observed [Fig. 3(d)] due to the suppression of I_c below the measurement resolution. The upper limit of I_c measured with voltage criteria V_c=0.2–0.5 μV is depicted by ×.

At $d_F^{0-\pi}$=2.95 nm the Josephson phase changes from 0 to π. There is no indication that another minimum occurs before, also not below 1 nm, as this is inside the dead magnetic layer regime (see Sec. III C). The maximum j_c in the π state is ~3.4 A/cm^2.

The $I_c(T)$ dependence of samples is shown in the vicinity and apart from the phase-transition thickness $d_F^{0-\pi}$ in Fig. 4 and insets of Fig. 3.

III. DISCUSSION

In this section we discuss the transport properties of our Ni film, the temperature-induced phase transition and compare our $j_c(d_F)$ data with clean and dirty limit theory. For discussion we used only the data from set 2, as set 1 contains less data, and its $j_c(d_F)$ dependence is similar to set 2, with lower amplitude of j_c.

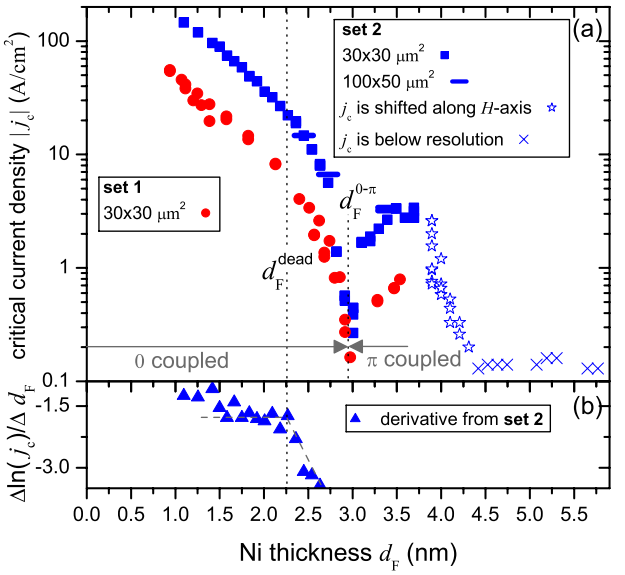

FIG. 2. (Color online) (a) $j_c(d_F)$ dependence for two sets of SIFS JJs. Set 1 has a thicker Al_2O_3 barrier than set 2. Standard $I_c(H)$ patterns were obtained, except for (i) samples with 73 having strongly shifted $I_c(H)$ pattern (see Ref. 16) and (ii) samples with thick d_F showing no $I_c(H)$ pattern, i.e., I_c is below the measurement resolution ×. The coupling changes from 0 to π at $d_F^{0-\pi}$ =2.95 nm. Measurements were taken at 4.2 K. (b) The dead magnetic layer regime is estimated by the change in slope of derivative of ln $j_c(d_F)$ as d_F^{dead}=2.26 nm. The dashed line in (b) is a guide for the eyes.

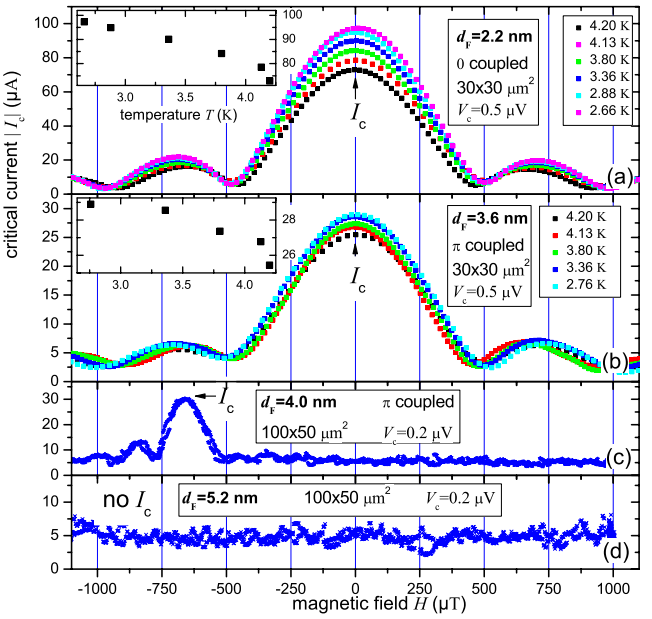

FIG. 3. (Color online) $I_c(H)$ dependence of JJs from set 2 for different thicknesses d_F. $I_c(T)$ for samples from (a) and (b) are plotted in the insets. Magnetic field was applied along the long axis of the 100×50 μm^2 samples. The strongly shifted $I_c(H)$ pattern from (c) is discussed in Ref. 16. (c) and (d) were measured at 4.2 K.

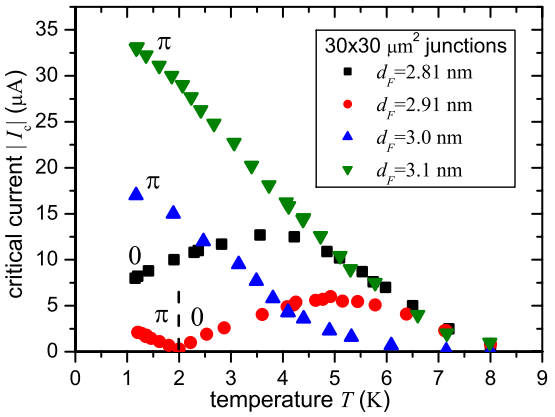

FIG. 4. (Color online) $I_c(T)$ dependence for JJs from set 2 in vicinity of the crossover thickness $d_F^{0-\pi}$. A temperature-induced 0 to π transition is observed (sample d_F=2.91 nm). $d_F^{0-\pi}$ is shifted from 2.95 nm (4.2 K) to 2.91 nm (2.0 K).

A. Mean-free path

The specific resistance ρ=7.4 $\mu\Omega$ cm at 4.2 K was determined by a four-point in-plane measurement of a 3.2 nm thin Ni film. However, one should consider the importance of grain-boundary scattering on the in-plane resistance for thin films. In the JJs current transport is out of plane, where ρ becomes smaller. The estimation of ℓ was problematic, as there is a considerable spread of data in the literature, depending strongly on the quality of Ni film. Assuming a constant Fermi surface and the Pippard relation[19] $\ell = \pi^2 k_B^2 / \gamma v_F e^2 \rho$ with a bulk specific-heat constant γ yields ℓ=3.3 nm, while considering the complex Fermi surface of Ni gives $\ell = 0.7-2.3 \times 10^{-15}$ $\Omega m^2/\rho = 9-30$ nm.[20] This estimation was confirmed by measurements of the out-of-plane length $\ell \approx 21$ nm (Ref. 21) for samples with in-plane specific resistance of ρ=3.3 $\mu\Omega$ cm, i.e., roughly half of our value. However, spin- and angle-resolved photoemissions[22] on some other Ni samples yield a spin-independent, very short mean-free path $\ell \approx 2$ nm.

The dirty limit condition $\ell < d_F$ is not valid over the total range of d_F=1–6 nm if considering the smaller values of ℓ, for larger values of ℓ it is not valid at all. To answer the question, whether our samples are in the clean or dirty limit, is not that easy. Therefore in Sec. III C we compare the $j_c(d_F)$ dependence both with clean and dirty limits Eq. (2) and Eq. (1).

B. Temperature dependence of I_c

In Fig. 4 the $I_c(T)$ dependence for four samples in the vicinity of the thickness-induced 0 to π transition is shown. By decreasing the temperature a 0 to π transition is observed for one sample (d_F=2.91 nm). The phase-transition thickness $d_F^{0-\pi}$ varies from 2.95 nm at 4.2 K down to 2.91 nm at 2.0 K. We present an observation of a T-induced 0 to π transition for SIFS junctions using an elemental magnet. Temperature induced 0 to π transitions were observed in dirty SFS stacks having transparent SF interfaces,[5] and theoretically predicted for clean SIFIS stacks.[15] For the dirty SIFS stacks, having one transparent SF interface, it was observed in NiCu-based JJs.[6] We are not aware of the experimental observation of temperature-induced 0 to π transition in presumably clean SFS, SIFS, or SIFIS stacks. Thus its occurrence in our Ni-SIFS stacks is an indication for being in the dirty limit condition and having one transparent SF interface.

The sample with d_F=2.81 nm in Fig. 4 shows an anomaly in $I_c(T)$ below 4.0 K, but does not change the ground state. For JJs with d_F over 0.2 nm from $d_F^{0-\pi}$ normal $I_c(T)$ dependencies were measured; see insets of Fig. 3.

In principle, one may try to fit the general form of $I_c(d_F, T)$ to the measured $I_c(T)$ dependencies. However, among parameters such as exchange energy E_{ex}, Fermi velocity v_F, spin-flip scattering time τ_m, and thickness d_F one should enter the mean-free path ℓ, which cannot be determined precisely for our samples.

C. *F*-layer thickness dependence of j_c

For smallest F-layer thicknesses d_F the JJs are supposed to be inside the dead magnetic layer regime, and JJs with thicker d_F should show a $j_c(d_F)$ dependence being influenced by the exchange energy. We split the data into different F-layer thickness regimes showing a dead magnetic layer, exchange, and exchange+anisotropy, denoted by I, II and III.

1. Nonmagnetic interlayer regime

Inside the dead magnetic layer 0 nm $< d_F < d_F^{\text{dead}}$ the wave-function amplitude is damped like in nonmagnetic normal metal. A dead magnetic layer can be caused by polycrystalline growth, interdiffusion at both interfaces (Cu or Nb), and the rather weak magnetic moment of Ni. The local magnetic moments are uncoupled, and have random orientations, i.e., the material is paramagnetic. In the literature[11] d_F^{dead} in SFS JJs with F=Ni was determined as 1.3 nm, indicating that its influence on the supercurrent transport is not negligible. In our case regime I ($d_F \leq d_F^{\text{dead}}$) covers JJs which show the normal proximity effect due to leakage of Cooper pairs in the dead magnetic layer,

$$j_c = j_c^0 \exp\left(\frac{-d_F}{\xi_F^{\text{dead}}}\right). \tag{3}$$

j_c^0 is the maximum amplitude without Ni layer, i.e., of a SINS junction. d_F^{dead} is estimated as 2.26 nm by the change in slope of $\Delta \ln(j_c)/\Delta d_F$; see Fig. 2(b). The dashed line serves as guide for the eyes. Fitting Eq. (3) to regime I of set 2 yields j_c^0=0.76 kA/cm^2 and ξ_F^{dead}=0.68 nm; see dotted line in Fig. 5. The measured value for a SINS-type junction (N=2 nm Cu) is j_c^0=4 kA/cm^2, indicating some additional scattering at the Ni interfaces of SINFS stack.

2. Clean limit

The clean limit Eq. (2) was fitted [Fig. 5(a)] to the data inside the magnetic regime, i.e., $d_F > d_F^{\text{dead}}$. We obtained an exchange energy E_{ex}=380 meV (solid line) assuming $v_F = 2.2 \times 10^5$ m/s.[22] However, this fit yields several minima in j_c, which cannot be seen in our set of data. For completeness we calculated $j_c(d_F)$ for E_{ex}=300 and 80 meV. Again, the

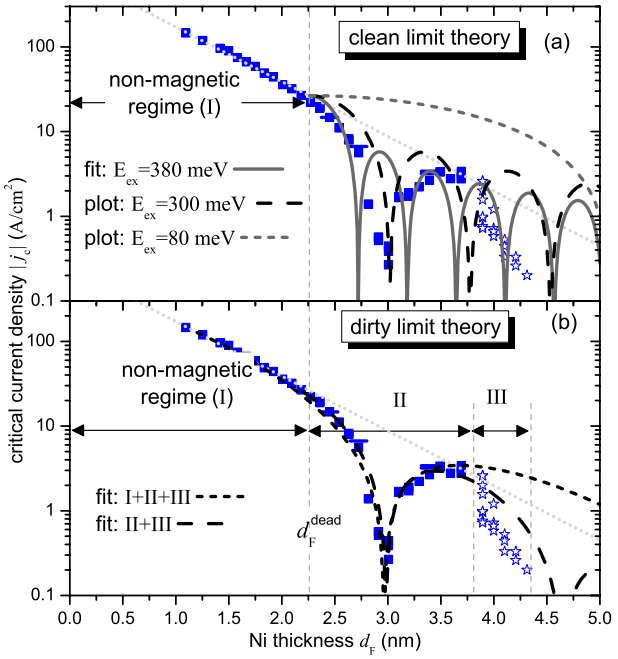

FIG. 5. (Color online) $j_c(d_F)$ dependence for set 2. The data set is split into different regimes: nonmagnetic (denoted by I), magnetic exchange (II) and magnetic exchange+anisotropy (III). The fit to regime I (dotted line) is extrapolated to the magnetically active regime. (a) The *clean* limit dependence [Eq. (2)] was fitted (solid line, yielding E_{ex}=380 meV) and plotted (dashed lines) for E_{ex} =80 and 300 meV. Starting F-layer thickness is d_F^{dead} for all three curves. (b) Two fits for *dirty* limit dependence [Eq. (1)] for data from regimes I+II+III and just II+III. For more details, see text.

agreement with data is bad. Our data have either a larger oscillation period or the decay length is shorter than for the calculated curve. One may increase d_F^{dead} to obtain a slightly better congruence, but at the same time the data set for fitting becomes even smaller.

We conclude that the clean limit theory Eq. (2) cannot reproduce our data. Furthermore, the strong decay of j_c inside dead magnetic regime can only be explained by dirty limit condition and after onset of magnetism in $d_F > d_F^{dead}$ the transport regime is not expected to modify drastically to the clean limit condition.

3. Dirty limit

Two fits were done for different data ranges in order to reproduce the experimental data, i.e., Eq. (1) was fitted to the total range (regimes I+II+III) and magnetic active range (II+III), respectively. We estimated ξ_{F1}=0.81(0.66) nm, ξ_{F2}=1.18(0.53) nm, and d_F^{dead}=1.2(2.26) nm.

For both fits (to I+II+III or II+III) we obtained a short decay length $\xi_{F1} \ll d_F$. The fit to I+II+III yields a rather large ξ_{F2}, strong decay ($\xi_{F1} < \xi_{F2}$), and underestimates the decay of j_c inside π state, whereas the fit to II+III has good correlation with data, but yields $\xi_{F1} > \xi_{F2}$, which, strictly speaking, contradicts the dirty limit theory.

Assuming the lowest value for the mean-free path, i.e., ℓ=2 nm,[22] the values for ξ_{F1}, ξ_{F2} gave

$$E_{ex} = \left(\frac{1}{\xi_{F1}} + \frac{1}{\xi_{F2}}\right)^2 \frac{\hbar v_F \ell}{12} = 104(279) \text{ meV}$$

and $\hbar/\tau_m$=0.37(0.22)E_{ex}. Larger values for ℓ yield an E_{ex} being much larger than the bulk value ($E_{ex} \approx 310$ meV). However, up to d_F^{dead}=2.26 nm no magnetic influence on j_c was observed, and the second dirty limit condition $\ell < \hbar v_F / E_{ex}$ was at least valid for very thin d_F, when E_{ex} was strongly reduced or even vanished. This conclusion is limited by the small range of data, which included the strongly shifted $I_c(H)$ pattern in regime III.

Thus, we state that the samples were dirty within the dead magnetic region. j_c of our Ni-SIFS samples considerably drops inside regime I by a factor of ~5 at the F-layer interface and $\sim e^{d_F^{dead}/\xi_F^{dead}} \approx 20$ inside the dead magnetic layer. If the analysis is limited to the magnetically active part (regimes II+III) indications for dirty limit conditions arise, too, although the set of data is rather small and $\xi_{F1} > \xi_{F2}$ cannot be explained by the theory for Eq. (1). For the clean limit condition we should observe some I_c for $d_F > 4.4$ nm. Its absence may be caused by the onset of magnetic anisotropy effects in regime III.

D. Comparison with literature

Compared to SFS JJs with Ni as an interlayer,[8–11] where multiple $I_c(d_F)$ oscillations were possibly observed, we can determine just one oscillation in our SIFS samples due to both the dirty transport regime and the onset of anisotropy. Our SIFS JJs, made by multilayer process, optical lithography, and ion etching, are good integratable into standard digital logics such as RSFQ logic. The FIB-patterned SFS JJs (Ref. 11) are not suitable for integration into complex circuits, and the SFS stacks made by Ref. 8–10 were not fabricated in one run, and some degree of irreproducibility during deposition or patterning may have occurred, leading to an increased spread of data. We regard our *in situ* multilayer deposition as being superior, especially regarding the quality of interfaces. Over and above for all SFS JJs just a few data points were obtained. For example, the oscillation period determined in early work[8] was later corrected[9,10] by samples with some closer spacing of d_F.

On one hand, our more sophisticated stacks—containing an Al_2O_3 tunnel barrier and a thin structural Cu layer—are subject to stronger scattering at the interfaces and therefore more likely to have a j_c below the measurement resolution. On the other hand our samples have very smooth lower SI interface, which is secured by the observation of tunneling. The local current density depends exponentially on tunnel barrier thickness, and a variation in Al_2O_3 thickness would provoke pinholes and magnetic-field-independent IV characteristics. The interface roughness is much smaller than the tunnel barrier thickness ≈1 nm. Our larger density of data than in Refs. 8–11 yields more information both on (i) the variation in j_c for same d_F (very low due to same run deposition and patterning) and (ii) the transport close to the onset of magnetism in F layer.

In Table I we give an overview on the current status on π coupled JJs being SFS or SIFS type. The rather high j_c of

TABLE I. Junction parameters of SFS and SIFS JJs showing magnetic interlayer thickness-dependent inversion of the ground-state phase. The j_c cannot be calculated from Ref. 11.

Magnet	Type	d_F^{dead} (nm)	$j_c(\pi)$ (A/cm^2)	$I_cR(\pi)$ (μV)	$I_cR_n(\pi)$ (μV)	T (K)	Dirty/clean	E_{ex} (meV)	Ref.
$Ni_{0.6}Cu_{0.4}$	SIFS	3.09	5	400	28	2.11	Dirty	99	6
$Ni_{0.53}Cu_{0.47}$	SFS	4.3	1000	0.15		4.2	Dirty	73	5
Ni	SIFS	2.26	3.4	7.3	3.7	4.2	Dirty	279	This work
Ni	SFS		1000	0.2		4.2	Clean	200	9 and 10
Ni	SFS	1.3		100		4.2	Clean	80	11
Co	SFS	0.8		60		4.2	Clean	309	11
Fe	SFS	1.1		125		4.2	Clean	256	11
$Ni_{0.8}Fe_{0.2}$	SFS	0.5		80		4.2	Clean	201	11
$Pd_{88}Ni_{12}$	SIFS		0.036		18	1.5	Dirty	201	4

SFS junctions is achieved by low interface scattering, and therefore they have a considerably lower junction resistance as the SIFS-type junctions.

The large amplitude of the subgap current, which depends on d_F and T, complicates the determination of the junction resistance. Usually for SIS junctions the normal state, Ohmic resistance R_n, measured beyond $V>2\Delta/e$ is considered for the quality factor. Current-biased SIFS JJs jump from the Meissner state to a voltage $V<2\Delta/e$ which depends on the subgap-resistance R. However, for SFS-type junctions $R_n=R$ is taken as the constant resistance branch for $I>I_c$ and at $V\ll\Delta/e$. For implementation of SIFS JJs the I_cR product is only relevant, too. In first work on SIFS JJs (Ref. 4) $I_cR_n(d_F)$ instead of $I_c(d_F)$ was used to avoid data scattering due to variations in R_n. However, in this paper R_n is constant for all JJs within an experimental error of about 5%, thus we plot $j_c(d_F)$.

The exchange energy for Ni and its Cu alloys is consistently ranging between 73 (Ref. 5) up to 279 meV (this work), except the considerable lower value in Ref. 11 for pure Ni (80 meV). Reference 11 does not provide information about the critical current density j_c, as the significant variation in junction area is overcome by considering just I_cR. One may speculate if these focused ion-beam etched JJs resemble more S(FN)S-type JJs,[23] where the interlayer consists of a ferromagnetic core being surrounded by a normal metal. This may explain the considerable lower exchange energy (80 meV, such as $Ni_{0.53}Cu_{0.47}$ alloy in Ref. 5) and the significant enhanced period of I_c oscillations ($\sim$4 nm).

SIFS junctions with Ni (this work) and NiCu (Ref. 6) as magnetic interlayer have similar j_c's, but R_n and I_cR_n of the NiCu based SIFS JJs are five times larger. The scattering probability in Ni and therefore the excess current are increased by this factor compared to NiCu alloys. Furthermore, the thicker Al_2O_3 barrier in NiCu SIFS JJs reduces the subgap current created by microshorts in the tunnel barrier, and provides a larger subgap resistance R.

We would like to point out that the use of Ni for π JJs has several disadvantages: (i) strong scattering of supercurrent, (ii) large dead magnetic layer where j_c is already reduced by a factor of 40, and (iii) anisotropy effects for $d_F>3.8$ nm. SIFS JJs with Co and Fe, having large atomic magnetic moments, may display anisotropy effects even for thinner magnetic thicknesses.

Based on the data of Table I the magnetically diluted Pd alloys may be an alternative for π SIFS JJs with high j_c, as the absolute drop of j_c due to F layer is only about a factor of 20–77.[4]

IV. CONCLUSIONS

In summary, SIFS JJs with a strong magnetic interlayer, i.e., Ni and an Al_2O_3 tunnel barrier were studied. Our samples had a large density of data points, ranging from the magnetically dead regime toward very thick d_F layers, being larger than in previous work on SFS JJs with elemental magnets,[8–11] where the data spacing was of the same order of magnitude as the phase oscillation lengths. Thus, we show results that allow to find the oscillation period for the elemental magnets reliably. The insertion of F layer leads to additional interface scattering compared to nonmagnetic junctions and inside the dead magnetic layer j_c drops exponentially. The dead magnetic layer thickness d_F^{dead} has been determined directly from transport measurements. The critical current I_c changes its sign as a function of the F-layer thickness d_F, exhibiting regions with 0 and π ground states. For d_F near the 0 to π crossover the ground state can be controlled by changing the temperature. This is an observation of a temperature-induced phase change using a strong magnet. For certain thicknesses the junctions show magnetic anisotropy effects, leading to a distortion of their $I_c(H)$ pattern. Overall, the transport regime is dirty, although locally inside the magnetically active F-layer regime a deviation from the strict dirty limit theory appears.

ACKNOWLEDGMENTS

The authors thank H. Kohlstedt, D. Sprungmann, E. Goldobin, D. Koelle, R. Kleiner, N. Pugach, M. Yu. Kupriyanov, and A. Palevski for stimulating discussions. J.P. was supported by Studienstiftung des Deutschen Volkes, V.S.S. and V.V.R. by the MOST-RFBR Project No. 06-02-72025 and M.W. by DFG Project No. WE 4359/1-1.

*m.weides@fz-juelich.de

[1] A. I. Buzdin, Rev. Mod. Phys. **77**, 935 (2005).
[2] V. V. Ryazanov, V. A. Oboznov, A. Y. Rusanov, A. V. Veretennikov, A. A. Golubov, and J. Aarts, Phys. Rev. Lett. **86**, 2427 (2001).
[3] H. Sellier, C. Baraduc, F. Lefloch, and R. Calemczuk, Phys. Rev. B **68**, 054531 (2003).
[4] T. Kontos, M. Aprili, J. Lesueur, F. Genet, B. Stephanidis, and R. Boursier, Phys. Rev. Lett. **89**, 137007 (2002).
[5] V. A. Oboznov, V. V. Bol'ginov, A. K. Feofanov, V. V. Ryazanov, and A. I. Buzdin, Phys. Rev. Lett. **96**, 197003 (2006).
[6] M. Weides, M. Kemmler, E. Goldobin, D. Koelle, R. Kleiner, H. Kohlstedt, and A. Buzdin, Appl. Phys. Lett. **89**, 122511 (2006).
[7] A. S. Vasenko, A. A. Golubov, M. Y. Kupriyanov, and M. Weides, Phys. Rev. B **77**, 134507 (2008).
[8] Y. Blum, A. Tsukernik, M. Karpovski, and A. Palevski, Phys. Rev. Lett. **89**, 187004 (2002).
[9] Y. Blum, M. Karpovski, V. Shelukhin, A. Palevski, and A. Tsukernik, *Future Trends in Microelectronics: The Nano, the Giga, and the Ultra* (Wiley Interscience/IEEE, New York, 2004), p. 270.
[10] V. Shelukhin, A. Tsukernik, M. Karpovski, Y. Blum, K. B. Efetov, A. F. Volkov, T. Champel, M. Eschrig, T. Löfwander, G. Schön, and A. Palevski, Phys. Rev. B **73**, 174506 (2006).
[11] J. W. A. Robinson, S. Piano, G. Burnell, C. Bell, and M. G. Blamire, Phys. Rev. B **76**, 094522 (2007).
[12] M. Weides, M. Kemmler, E. Goldobin, H. Kohlstedt, R. Waser, D. Koelle, and R. Kleiner, Phys. Rev. Lett. **97**, 247001 (2006).
[13] M. Weides, C. Schindler, and H. Kohlstedt, J. Appl. Phys. **101**, 063902 (2007).
[14] J. Pfeiffer, M. Kemmler, D. Koelle, R. Kleiner, E. Goldobin, M. Weides, A. K. Feofanov, J. Lisenfeld, and A. V. Ustinov, Phys. Rev. B **77**, 214506 (2008).
[15] Z. Radović, N. Lazarides, and N. Flytzanis, Phys. Rev. B **68**, 014501 (2003).
[16] M. Weides, Appl. Phys. Lett. **93**, 052502 (2008).
[17] M. Weides, K. Tillmann, and H. Kohlstedt, Physica C **437-438**, 349 (2006).
[18] H. Kohlstedt, F. König, P. Henne, N. Thyssen, and P. Caputo, J. Appl. Phys. **80**, 5512 (1996).
[19] A. B. Pippard, Rep. Prog. Phys. **23**, 176 (1960).
[20] C. Fierz, S.-F. Leet, J. Bass, W. P. Pratt Jr., and P. Schroeder, J. Phys.: Condens. Matter **2**, 9701 (1990).
[21] C. E. Moreau, I. C. Moraru, N. O. Birge, and W. P. Pratt, Appl. Phys. Lett. **90**, 012101 (2007).
[22] D. Y. Petrovykh, K. N. Altmann, H. Höchst, M. Laubscher, S. Maat, G. J. Mankey, and F. J. Himpsel, Appl. Phys. Lett. **73**, 3459 (1998).
[23] T. Y. Karminskaya and M. Y. Kupriyanov, JETP Lett. **85**, 286 (2007).